ADVANCED FUNCTIONAL MATERIALS
www.afm-journal.de

Tuning Molecular Adhesion via Material Anisotropy

Wenliang Zhang, Yuan Lin, Jin Qian, Weiqiu Chen,* and Huajian Gao*

Cell adhesion with extracellular matrix depends on the collective behaviors of a large number of receptor-ligand bonds at the compliant cell-matrix interface. While most biological tissues and structures, including cells and extracellular matrices, exhibit strongly anisotropic material properties, existing studies on molecular adhesion via receptor-ligand bonds have been largely limited to isotropic materials. Here the effects of transverse isotropy, a common form of material anisotropy in biological systems, in modulating the adhesion behavior of a cluster of receptor-ligand bonds are investigated. The results provide a theoretical basis to understand cell adhesion on anisotropic extracellular matrices and to explore the possibility of controlling cell adhesion via anisotropy design in material properties. The combined analysis and simulations show that the orientation of material anisotropy strongly affects the apparent softness felt by the adhesive bonds, thereby altering their ensemble lifetime by several orders of magnitude. An implication of this study is that distinct cellular behaviors can be achieved through remodeling of material anisotropy in either extracellular matrix or cytoskeleton. Comparison between different loading conditions, together with the effects of material anisotropy, yields a rich array of out-of-equilibrium behaviors in the molecular interaction between reactant-bearing soft surfaces, with important implications on the mechanosensitivity of cells.

1. Introduction

Specific molecular adhesion mediated by receptor-ligand bonds has attracted a growing number of researchers in recent years. In contrast to non-specific adhesion based on van der Waals type of interactions, molecular adhesion is intrinsically stochastic and its strength strongly depends on the mechanical properties of neighboring matrices. There is now ample experimental evidence showing that substrate stiffness plays important to crucial roles in receptor-ligand mediated cellular adhesion in processes such as cell spreading, migration, growth and differentiation.[1–5] A thorough understanding of stiffness-dependent molecular adhesion may open new opportunities in designing artificial materials to quantitatively control cellular behaviors, as demonstrated in experiments over different types of polyacrylamide- and alginate-based gels during the past two decades.[6,7]

The role of extracellular rigidity in cell-matrix interaction has been subjected to extensive theoretical and experimental efforts. For example, a recent study by Chan and Odde investigated matrix rigidity sensing of neuronal filopodia via a stochastic "motor-clutch" force transmission system.[8] Walcott and Sun considered the coupling between focal adhesion impedance against myosin-driven contractility and actin cytoskeleton reorganization under force, showing that the stiffness of substrate directly influences differential formation of stress fibers in cytoskeleton and ultimately leads to changes in intracellular biochemistry.[9] By developing a stochastic-elasticity framework, Qian and co-workers showed that matrix compliance has two detrimental effects on the stability and lifetime of molecular bond clusters: it induces severe stress concentration at the adhesion rim, leading to crack-like failure from the edges,[10,11] and also increases local separation between cell and substrate wherever debonding occurs, making it difficult to reform adhesion.[12] These existing theories on multivalent receptor-ligand adhesion, together with the key experiments studying stiffness effects on cellular behaviors,[1–5] have been largely limited to isotropic materials, with homogeneous or gradient stiffness described by a single modulus, overlooking the fact that most cell-bearing matrices and tissues exhibit strongly anisotropic material properties due to microstructural features such as ordered arrays of collagen fibrils.[13–15] From an engineering point of view, a variety of possible approaches to achieving control of cell-matrix adhesion via materials design still remain unexplored, including materials anisotropy, heterogeneity, composition, porosity, etc. With an aim to understand adhesive interactions between cells and extracellular matrices with native anisotropy and to inspire appropriate mechanical designs of synthetic functional materials, here we make the first theoretical attempt to investigate the effects of elastic anisotropy on receptor-ligand adhesion. Such effects have been

W. Zhang, Prof. J. Qian, Prof. W. Chen
Department of Engineering Mechanics
Zhejiang University
Hangzhou, Zhejiang 310027, China
E-mail: jqian@zju.edu.cn; chenwq@zju.edu.cn
Prof. Y. Lin
Department of Mechanical Engineering
The University of Hong Kong
Hong Kong, China
Prof. H. Gao
School of Engineering
Brown University
Providence, RI 02912, USA

DOI: 10.1002/adfm.201300069

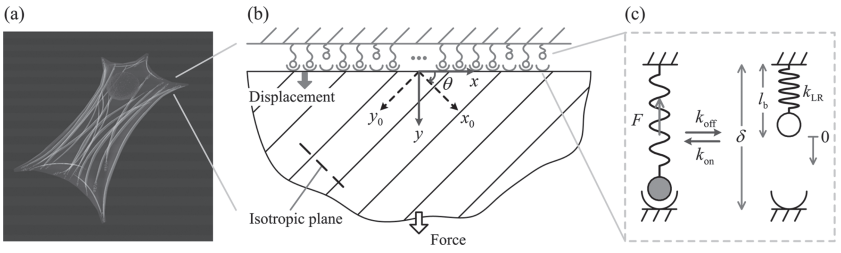

Figure 1. Schematic representation of the model. a) A cell adhered to an extracellular matrix, with transverse isotropy in its mechanical properties, through focal adhesions. The fibrous structure of cytoskeleton suggests that the intracellular environment may be resembled by a transversely isotropic material as well. b) An idealized theoretical model where a cluster of receptor-ligand bonds with finite size join a transversely isotropic half-space and a plate, subjected to a remotely applied force or a uniform displacement at the interface. The plate is assumed to be rigid due to the reflective symmetry without loss of generality. c) Bond transition between closed and open states at force-dependent dissociation and separation-dependent association rates.

previously shown to play significant roles in nonspecific van der Waals interaction.[16,17]

Transverse isotropy represents a relatively simple but important class of anisotropic materials with axisymmetry about a particular material axis and 5 independent elastic constants.[13,18] At certain scales, brain,[19] cortical bone[20] and skeletal muscle[21] tissues could all be adequately modeled as transversely isotropic materials, rooted in their fibrous structures at microscopic scales. The attachment pad of some insects (e.g., cicada) presents a smooth outer membrane with inner material made of transversely isotropic foams.[22] For the intracellular side of cell-matrix adhesion, it is not unreasonable to believe that the cytoskeleton consisting of unidirectional stress fibers bears some resemblance to the mechanical behavior of transversely isotropic materials.[23] Recent progress in various fabrication techniques has also led to highly controlled elastic anisotropy in synthetic composite materials by employing fiber-based architecture.[24–26] A comprehensive study of molecular adhesion to anisotropic materials should be of substantial interest to future development of biomimetic materials and devices for controlling cellular adhesion and related behaviors.

In this paper, we consider the molecular adhesion between a cell and an extracellular matrix, which bear native or synthetic transverse isotropy in their mechanical properties (**Figure 1**a). The interfacial adhesion is mainly achieved by the formation of contact sites, commonly referred to as focal adhesions, where a number of ligand-receptor bonds bring cell and matrix together. These bonds are laterally reinforced by a layer of protein complex including vinculin and paxillin, often referred to as an adhesion plaque, which interconnects ligand-receptor bonds into clusters and then attaches to the cytoskeleton of cells through stress fibers mainly consisting of actin filaments and myosin motors.

Any modeling on cell-matrix interaction has to involve the loading condition maintained at the focal adhesion sites. To date, whether it is the constant level of force or deformation that limits the cellular tractions between cell and extracellular environment is still a subject of debate.[27,28] There exist experimental studies suggesting that cells establish the traction forces at focal adhesions to maintain a level of constant stress.[27] However, other measurements have shown that cells exert traction forces on substrates in proportion to the substrate rigidity:[28] based on a simple mechanical analysis, constant average displacement is implied as the enforced loading condition at the cell-matrix interface. Because the precise mechanisms that govern the force regulation at focal adhesions are not yet fully understood, we proceed by representing the loading condition that is maintained at cell-matrix interface by two different cases, where constant load versus displacement is imposed to the molecular adhesion of receptor-ligand bond clusters.

We start with a brief description of stochastic bond breaking and reforming at molecular scale, as well as deformation of a transversely isotropic half-space in response to point forces using the explicit formalism of Barnett-Lothe tensors.[29] We demonstrate the effects of material anisotropy on molecular adhesion by considering a semi-infinite transversely isotropic body joining a rigid plate via a cluster of molecular bonds. For a given configuration of bond cluster, we adopt a discrete form of elastic Green's function approach to solve the non-uniform traction and displacement fields along the interface. The solutions to interfacial displacements and tractions are then used to determine the reaction rates and temporal evolution of molecular bonds in the cluster. Monte Carlo simulations are performed to investigate the effects of material anisotropy on the cluster lifetime and stability. We observe that the lifetime of molecular bond cluster exhibits very different trends of dependence on material anisotropy orientation under force- and displacement-control loading conditions, which have also been shown to have profound effects on cell re-alignment in response to cyclically stretched substrates.[30,31]

2. Model

Consider a cluster of molecular bonds of size $2a$ linking two media together against an externally applied tensile force far from the adhesion region, or a uniform interfacial displacement tending to separate the opposing surfaces, which approximates the possible loading condition maintained at focal adhesions between cell and extracellular matrix (Figure 1b). Without loss of generality, the lower material below adhesion is assumed to be transversely isotropic and the upper material rigid. The problem is treated as plane strain so that only a slice of material with thickness b equal to the bond spacing needs to be explicitly accounted for.

2.1. Biochemical Reactions of Molecular Bonds

There exist two competing processes governing the behavior of an adhesive receptor-ligand bond cluster. Each bond, owing to its low binding energy typically on the order of k_BT, where k_B is the Boltzmann constant and T is the ambient temperature in Kelvin), can reversibly transform between the open (detached) and closed (attached) states in a stochastic manner. Following

the pioneering model by Bell,[32] the rupture process of a closed bond can be regarded as a thermally assisted escape from a bound energy minimum over a transitional activation barrier in a one-dimensional energy landscape, with the rupture rate

$$k_{\text{off}} = k_0 \exp\left(\frac{F_{\text{bond}}}{F_{\text{b}}}\right) \tag{1}$$

exponentially depending on the force F_{bond} acting on the bond. Here, the coefficient k_0 is the spontaneous rate of bond rupture at zero force, and $F_{\text{b}} = k_{\text{B}}T/x_{\text{b}}$ is recognized as an intrinsic force scale that causes e-fold increase in rupture rate, with x_{b} representing a characteristic distance between the bound energy minimum and the transitional activation barrier. Equation 1 implies that the pulling force F_{bond} only tilts the height of the activation barrier without biasing its distance to the energy minimum. For typical receptor-ligand bonds in cell adhesion, $1/k_0$ is found to fall in the range from a fraction of a second to 100 s and x_{b} is on the order of 1 nm, depending on bond types.[33]

The long-term stability of a multiple-bond cluster is attributed to the so-called clustering size effect of bond cooperation, where any broken bond can rebind before the whole adhesion ensemble fails.[34,35] The rebinding (or association) process of an open bond is characterized by reaction rate k_{on}. Suppose a broken pair of receptor and ligand can rebind at a constant rate $k^0{}_{\text{on}}$ when they are held within a binding distance l_{bind} in close proximity; when they are apart beyond the binding distance, the receptor has to first approach the binding spot of the ligand through Brownian motion. We further assume for simplicity that the ligand is fixed on the substrate surface while the receptor is tethered to the opposing cell surface by a linear spring of stiffness k_{LR} and rest length l_{b} (Figure 1c). At this point, the probability density function of the distance between the two binding ends can be obtained according to the Maxwell-Boltzmann distribution. As such, the association rate of the open bond can be written as a function of the separation δ between the two surfaces, where the ligand and receptor are anchored, in the following form:[36,37]

$$k_{\text{on}} = k^0_{\text{on}} \frac{l_{\text{bind}}}{Z} \exp\left(-\frac{k_{\text{LR}}(\delta - l_{\text{b}})^2}{2k_{\text{B}}T}\right) \tag{2}$$

where Z is the partition sum for the receptor confined in a truncated harmonic potential between $-l_{\text{b}}$ and $\delta - l_{\text{b}}$ (Figure 1c). Not surprisingly, the association rate described above strongly depends on the separation distance between the opposing receptor and ligand, and the binding reaction becomes hardly possible once the open pair of bonds are apart beyond a threshold value.

2.2. Barnett–Lothe Tensors for Transversely Isotropic Materials

Transversely isotropic materials, as a special type of anisotropic materials, can be used to represent many biological tissues with fibrous microstructures.[19–21] The mechanical properties of transversely isotropic materials are isotropic in a particular plane, denoted as (x_0,z_0) plane in the present study (Figure 1b), but significantly different along the direction perpendicular to the isotropic plane, i.e. the symmetry axis denoted as y_0 direction. Structurally, the symmetry axis y_0 often indicates the dominating orientation of the microscopic fibers. The elastic properties of a transversely isotropic material are fully characterized by five independent constants: Young's modulus E_1 and Poisson's ratio ν_1 in the isotropic (x_0,z_0) plane; Young's modulus E_2 in the y_0 direction and Poisson's ratio ν_2 describing the transverse contraction in the isotropic plane due to an applied stress parallel to y_0; shear modulus G_{12} in any plane parallel to the symmetry axis.

The 2D elasticity problems in anisotropic solids have been widely studied using the so-called Stroh formalism and Barnett-Lothe tensors.[29] For transversely isotropic materials, the Barnett-Lothe tensors can be deduced from those for orthotropic materials as[38]

$$\mathrm{S_o} = \begin{bmatrix} 0 & s_{12} \\ s_{21} & 0 \end{bmatrix},\ \mathrm{L_o} = \begin{bmatrix} L_{11} & 0 \\ 0 & L_{22} \end{bmatrix} \tag{3}$$

where

$$s_{12} = -\alpha_2\gamma_1\chi_1, s_{21} = \alpha_1\gamma_2\chi_1, L_{11} = \alpha_1\gamma_1 E_1, L_{22} = \alpha_2\gamma_2 E_2 \tag{4}$$

are defined through a group of parameters as

$$\begin{aligned}
\gamma_1 &= \left(E_1/G_{12} + 2\chi_1\sqrt{E_1/E_2}\right)^{-1/2}, \\
\gamma_2 &= \left(E_2\Big/G_{12} + 2\chi_1\sqrt{E_2/E_1}\right)^{-1/2}, \\
\alpha_1 &= \left(1-\nu_1^2\right)^{-1/2}, \alpha_2 = \left(1 - \frac{\nu_2^2 E_1}{E_2}\right)^{-1/2}, \\
\chi_1 &= \sqrt{\left(1-\nu_1^2\right)\left(1 - \frac{\nu_2^2 E_1}{E_2}\right)} - (1+\nu_1)\,\nu_2\sqrt{\frac{E_1}{E_2}}
\end{aligned} \tag{5}$$

Note that L_{11} and L_{22} have the same dimension as Young's moduli E_1 and E_2, and s_{12} and s_{21} are dimensionless quantities. The Poisson's ratio for most materials ranges between zero and a half, and hence α_1 and α_2 are both constants close to unity recognizing $E_1/E_2 < 1$. One can show that

$$\frac{L_{11}s_{12}}{L_{22}s_{21}} = -1 \tag{6}$$

2.3. Elastic Response of a Transversely Isotropic Half-Space to Point Force

Now we examine the elastic response of a transversely isotropic half-space when its surface is subjected to an arbitrarily distributed traction. As pointed out earlier, we explore the solution under plane strain conditions. The Barnett–Lothe matrices **S** and **L**, defined in the coordinate system (x,y) that is chosen to be parallel and perpendicular to the half-space surface and deviates from the material frame (x_0,y_0) with a rotation angle θ, can be calculated from their counterparts in Equation 3 through the following transformations:

$$\mathbf{S} = \Omega \mathbf{S}_0 \Omega^{\mathrm{T}}, \mathbf{L} = \Omega \mathbf{L}_0 \Omega^{\mathrm{T}} \tag{7}$$

where the superscript T denotes matrix transposition and the transformation tensor

$$\Omega_o = \begin{bmatrix} \cos\theta & -\sin\theta \\ \sin\theta & \cos\theta \end{bmatrix} \tag{8}$$

accounts for the rotation between the two coordinate systems.

The surface displacements of the transversely isotropic half-space, denoted as $\mathbf{u} = [u_x\ u_y]^T$, are related to surface traction $\mathbf{p} = [p_x\ p_y]^T$ through the following integral equation of vector form:[29]

$$\frac{1}{\pi}\int_{-\infty}^{\infty} \frac{\mathbf{L}^{-1}}{s-x}\mathbf{p}(s)\,\mathrm{d}s + \mathbf{S}\mathbf{L}^{-1}\mathbf{p}(x) = \frac{\partial \mathbf{u}}{\partial x} \tag{9}$$

In the present study, $\mathbf{p}$ represents the force exerted by a single bond and thus is specified to be a tensile traction normal to the surface, which is postulated to be uniformly distributed over the bond region $2a_0$, a_0 being the radius of the bond (**Figure 2**a). In other words,

$$\mathbf{p} = \begin{bmatrix} 0 & p_y(x) \end{bmatrix}^{\mathrm{T}} \tag{10}$$

where p_y is equal to -p for $|x| \le a_0$ and zero otherwise, p representing the magnitude and the negative sign accounting for the direction.

Substituting Equations 7 and 10 into Equation 9, the x-component of the equation regarding the tangential displacement u_x has negligible effects in contributing to surface settlement in normal direction, and the y-component becomes

$$\frac{C_1}{\pi}\int_{-a_0}^{a_0} \frac{p_y(s)}{s-x}\mathrm{d}s + C_2 p_y(x) = \frac{\partial u_y(x)}{\partial x} \tag{11}$$

where

$$C_1 = \frac{\cos^2\theta}{L_{22}} + \frac{\sin^2\theta}{L_{11}},\ C_2 = \frac{(L_{11}s_{12} + L_{22}s_{21})\sin 2\theta}{2L_{11}L_{22}} \tag{12}$$

Recalling Equation 6 that $L_{11}s_{12} + L_{22}s_{21} = 0$, C_2 vanishes and thus the normal surface displacement u_y is symmetric with respect to the center of the loaded region. It should be pointed out that the emergence of Equations 11 and 12 relies on the simplification that the surface traction $\mathbf{p}$ has zero component in tangential direction, which is the case for current study of normal tensile bond force. The reader is encouraged to consult various studies for more general cases where both normal and tangential tractions are significant.[16,17,39]

Integrating Equation 11 with respect to x leads to

$$u_y(x) = \frac{C_1}{2\pi}p\left\{\begin{array}{l}(x+a_0)\ln\left(\frac{x+a_0}{a_0}\right)^2 \\ -(x-a_0)\ln\left(\frac{x-a_0}{a_0}\right)^2 + c_\infty\end{array}\right\} \tag{13}$$

where c_∞ is a length constant chosen to satisfy the condition that the bond traction $p_y(x)$ causes zero displacement at a reference point x_∞. Throughout the following analysis, $x_\infty/a_0 = 10^4$ is chosen for a datum far from the bond. Figure 2b shows the profile of the deformed surface for several values of the anisotropy orientation angle θ, where $L_{22}/L_{11} = 4.4$ is taken from experimentally measured material parameters for muscle tissues: E_1 = 20 kPa, E_2 = 450 kPa, $\nu_1 = \nu_2$ = 0.375 and G_{12} = 4 kPa.[21,40] The figure shows that the magnitude of the surface deformation increases as θ varies from zero to $\pi/2$, which can be readily understood from the elevated material compliance in the transverse direction of muscle fibers.

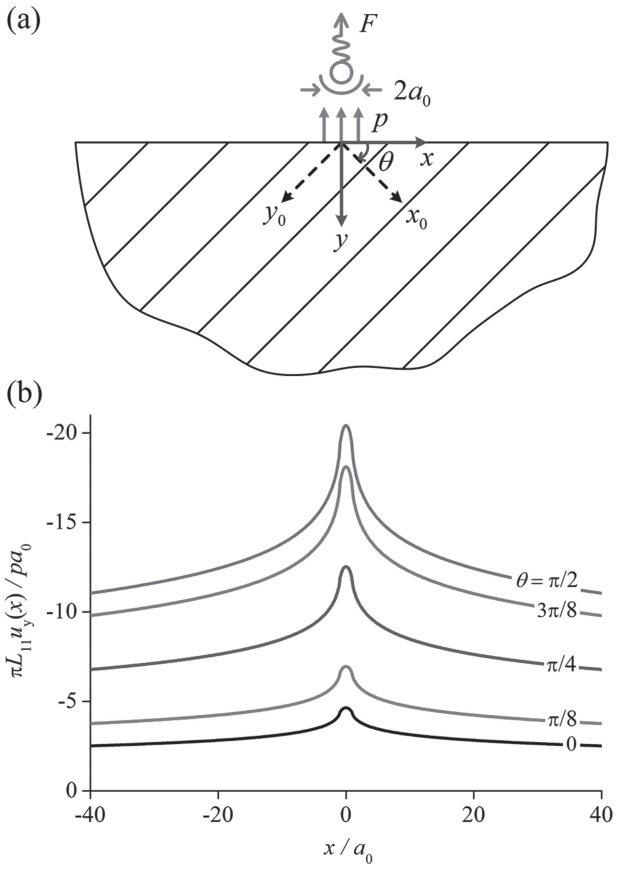

Figure 2. Elastic response of a transversely isotropic half-space to single bond forces. a) A normal tensile traction p, uniformly distributed over a strip with width $2a_0$, is applied on the surface of the transversely isotropic half-space. The anisotropy orientation is represented by the angle θ between the half-space surface and the isotropic plane of the transversely isotropic material. b) The profiles of the deformed surface for several values of the anisotropy orientation angle θ. The involved parameter in (b) is $L_{22}/L_{11} = 4.4$, based on the reported values for muscle tissues.[21,40]

Comparing Equation 13 to the corresponding result for isotropic materials,[41] one can see that the anisotropic substrate behaves as an effective isotropic material with Young's modulus E^* determined through

$$\frac{1}{E^*} = \frac{1}{2}\left(\frac{\cos^2\theta}{L_{22}} + \frac{\sin^2\theta}{L_{11}}\right) \tag{14}$$

E^* varies between two limiting values, $2L_{11}$ and $2L_{22}$, depending on the anisotropy orientation angle θ (**Figure 3**). Clearly,

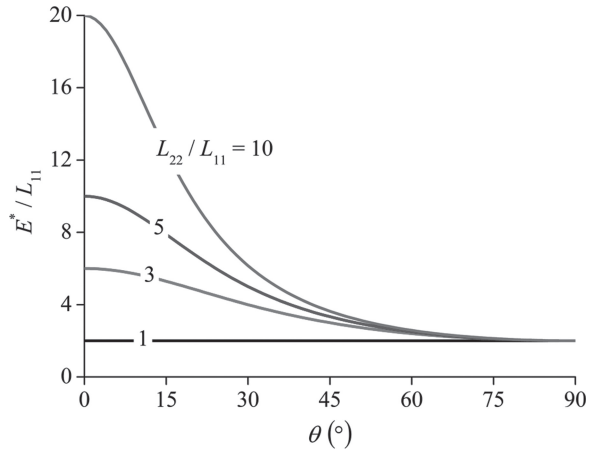

Figure 3. Effective modulus of the transversely isotropic half-space, denoted as E^*, as a function of the anisotropy orientation angle θ.

$$E^*(\theta) = E^*(\pi \pm \theta) \tag{15}$$

for any specified values of L_{22}/L_{11}, so the following discussion is made for θ ranging between zero and $\pi/2$.

When both the intracellular fibrous network within a cell and the extracellular matrix to which the cell attaches possess transverse isotropy (Figure 1a), the cell-matrix adhesion problem can be equivalently converted to the "master" problem in Figure 1b, where the upper material is rigid and the lower one has the effective modulus E^* determined through

$$\frac{1}{E^*} = \frac{1}{2}\left(\frac{\cos^2\theta^{(1)}}{L_{22}^{(1)}} + \frac{\sin^2\theta^{(1)}}{L_{11}^{(1)}}\right) + \frac{1}{2}\left(\frac{\cos^2\theta^{(2)}}{L_{22}^{(2)}} + \frac{\sin^2\theta^{(2)}}{L_{11}^{(2)}}\right) \tag{16}$$

according to a typical treatment for interfacial adhesion problems.[41] Here θ, L_{11} and L_{22} follow the definitions described above, and the superscripts 1 and 2 denote the cell and the matrix, respectively.

2.4. Green's Function Approach for an Array of Discrete Bonds

We now extend the analysis to an arbitrarily distributed array of bond forces acting on the half-space surface, as described in Figure 1b for multiple-bond adhesion. The bond j in the cluster induces a force F_j, defined positive under tension, on the surface of the transversely isotropic medium. Again, the bond force is regarded as a uniformly distributed traction p_j over the region $2a_0$ occupied by a single bond. For self-consistency, we must have

$$p_j = F_j/2a_0b \tag{17}$$

for the adopted plane strain configuration (Figure 1b). The normal displacement u_y of the surface at a bond location x_i induced by the force F_j at location x_j can be written in terms of a Green's function G_{ij} as:

$$u_y(x_i, x_j) = G_{ij}F_j \tag{18}$$

where

$$G_{ij} = \frac{C_1}{4\pi a_0 b}\left\{\begin{array}{l}(x_i - x_j + a_0)\ln\left(\frac{x_i - x_j + a_0}{a_0}\right)^2 \\ -(x_i - x_j - a_0)\ln\left(\frac{x_i - x_j - a_0}{a_0}\right)^2 + c_\infty\end{array}\right\} \tag{19}$$

in consistency with Equation 13.

As illustrated in the upper portion of **Figure 4**, for those sites where the bonds are closed, the compatibility condition is that the stretched bond length subtracting the normal displacement of the surface should be equal to the nominal separation of the interface, denoted as h, i.e.,

$$\frac{F_i}{k_{LR}} + l_b - \sum_{j=1}^{k} G_{ij}F_j = h \tag{20}$$

where k is the number of closed bonds in the adhesion region at an instant. As long as there are bonds remaining unbroken

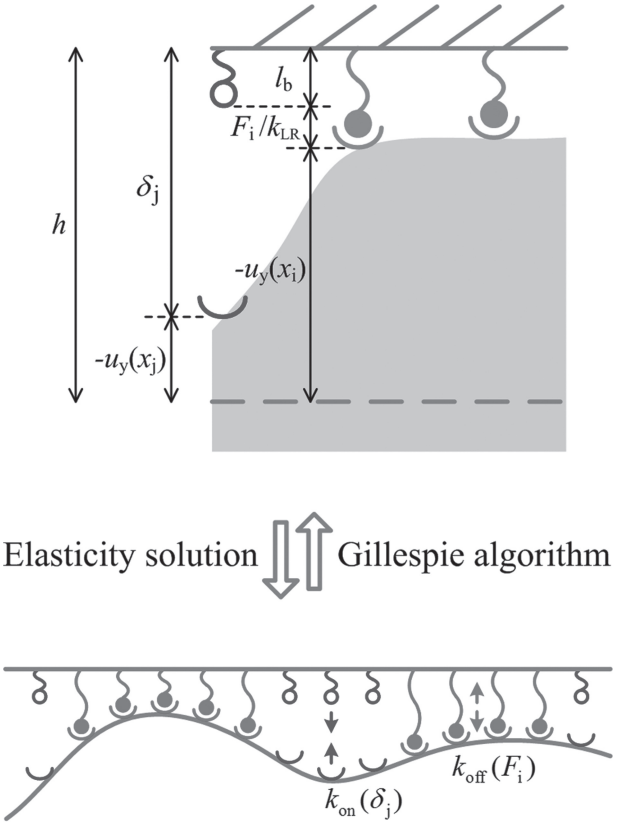

Figure 4. Stochastic-elasticity coupling in the modeling framework that unifies elastic field descriptions of bond force and interfacial separation, and stochastic descriptions of discrete rupture and rebinding processes in a bond cluster. The elasticity solution is based on the compatibility condition at the interface, where the stretched length of individual bonds, $l_b + F_i/k_{LR}$, subtracting local normal displacement u_y of the surface should be equal to a constant separation h for all the closed bonds. The determination of bond reaction to occur is sampled among all the bonds according to their association (k_{on}) or dissociation (k_{off}) rates using the Gillespie algorithm.

(i.e., $k > 0$), they will be stretched in the loading direction and the global force balance implies

$$\sum_{i=1}^{k} F_i = F \tag{21}$$

where F is the total force applied to the molecular adhesion.

For the loading condition of a constant F, the so-called force-control loading, the nominal interfacial separation h, i.e., the interfacial gap without surface deformation, is unknown and should be part of the solution. The unknown vector (F_1, F_2, ..., F_k, h) can be determined through the $k + 1$ equations in Equations 20 and 21. On the other hand, under displacement-control loading condition where a constant h is maintained during the whole process, the $k + 1$ unknowns become (F_1, F_2, ..., F_k, F), which are to be solved from Equations 20 and 21.

Referring to Figure 4 (upper portion), the separation δ_j between the deformed surfaces at the open bond j depends on forces on all other unbroken bonds and the initial separation h as

$$\delta_j = h + \sum_{i=1}^{k} G_{ji} F_i \tag{22}$$

Once all the forces on closed bonds and all the surface separations at open bonds are obtained, we can calculate the reaction (rupture or rebinding) rates of all bonds during the temporal evolution of a molecular bond cluster.

2.5. Stochastic-Elasticity Coupling

To implement the stochastic-elasticity coupling in the spatial and temporal evolutions of all bonds along the interface, we make use of the 'first reaction method' derived from the Gillespie algorithm to sample random trajectories of the system.[42,43] Specifically, each bond within the adhesion cluster, open or closed, is treated as an independent reaction site as indicated in the lower portion of Figure 4. The reaction times at individual bonds are calculated for the corresponding rupture and rebinding events according to

$$\tau_i = -\frac{\ln \xi_i}{\mu_i} \tag{23}$$

where i refers to individual bonds, ξ_i are a series of random numbers independently drawn from a uniform distribution over the unit interval [0, 1], and μ_i are the calculated rupture or rebinding rates depending on the bond status at site i. The actual reaction to take place and the corresponding reaction time are determined to be the shortest one, denoted as τ_{min}, among those obtained from Equation 23. With the selection, the simulation time marches forward by τ_{min}, and the reaction site where τ_{min} is selected should flip its bond state from closed to open or vice versa. This change of bond state requires an update in the bond force distribution, as well as the interfacial separation, which can then be used to determine reaction rates at the next time step.

Figure 4 shows the adopted procedure of calculating imaginary reaction times, selecting actual reaction, advancing simulation time, executing changes in bond state and computing reaction rates from an updated configuration. This loop repeats until all the bonds within the cluster become open, a state regarded as failure of the whole adhesion in our study. The cumulative simulation time is then recorded as the cluster lifetime. For any given set of model parameters, we independently perform the simulation for 1000 times, a number found to adequately ensure meaningful statistics. The averaged value of lifetime, normalized by time scale $1/k_0$ and denoted as τ_T, is then calculated and serves as a direct measure of cluster stability.

3. Results and Discussion

3.1. Estimate of Parameters

Now we examine the lifetime and stability of a cluster of N_T = 100 adhesive bonds evenly distributed at a spacing of b = 32 nm, which corresponds to a typical bond density of ≈1000 per μm^2. The size of the adhesion cluster considered here is around 3.2 μm, similar to the characteristic size of focal adhesions.[44,45] The stiffness and rest length of individual bonds are taken to be k_{LR} = 0.25 pN/nm and l_b = 11 nm, respectively, which are typical estimates for fibronectin/integrin bonds.[37] The radius of a single bond is chosen as a_0 = 5 nm in light of the fact that the diameter of integrin molecules is estimated to be around 10 nm.[46] The bond spacing we use, 32 nm that corresponds to ≈1000 per μm^2, is a typical value for integrin-based focal adhesions. Experiments have revealed that stable focal adhesions are only formed for bond spacing 58 nm and less, and the achievable density of close-packed receptors corresponds to a minimum bond spacing of 10 nm, which is the size of integrin molecules.[46] Moreover, these limiting values of bond spacing, 10 nm and 58 nm, have been confirmed to be universal across

Table 1. Model parameters.

Parameter	Definition	Value	Ref.
E_1	Young's modulus in the isotropic plane	20 kPa	[21]
E_2	Young's modulus in out-of-plane direction	450 kPa	[21]
ν_1, ν_2	Poisson's ratio	0.375	[40]
G_{12}	Out-of-plane shear modulus	4 kPa	[21]
N_t	Number of total bonds in a molecular cluster	100	[44,45]
b	Spacing between neighboring bonds	32 nm	[46]
a	Half-width of a bond cluster	1.6 μm	[44]
k_{LR}	Stiffness of individual bonds	0.25 pN/nm	[37]
l_b	Rest length of individual bonds	11 nm	[37]
a_0	Radius of individual bonds	5 nm	[46]
F_b	Force scale in Bell's dissociation model	4 pN	[33]
l_{bind}	Binding radius of receptor-ligand pairs	1 nm	[36]
k_{on}^0/k_0	Normalized bond association rate within l_{bind}	10^4	[36]
k_BT	Unit of thermal energy	4.1 pN nm	Constant

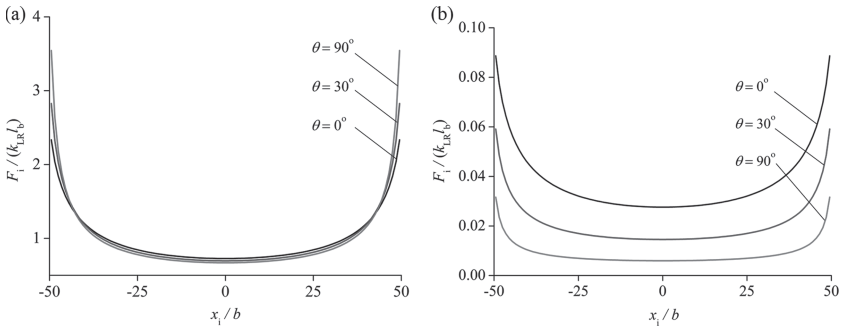

Figure 5. Distributions of the normalized bond force at different values of the anisotropy orientation angle θ for two types of loading conditions. a) For force-control systems, the distribution of interfacial traction among bonds can be modulated through anisotropy orientation that controls the effective substrate stiffness, as understood by the concept of stress concentration index[10,11] (applied constant force: $F = N_T k_{LR} l_b$). b) For displacement-control systems, in addition to the extent of concentrated distribution of bond forces, a more important effect of anisotropy orientation is to modulate the averaged level of bond force (applied constant displacement: $h = 2l_b$).

cell types including fibroblast, osteoblast and melanocyte.[46] The selected bond spacing in the present study is between the two limits. Based on the reported data on muscle tissues, the transversely isotropic material constants are taken as E_1 = 20 kPa, E_2 = 450 kPa, $\nu_1 = \nu_2 = 0.375$ and G_{12} = 4 kPa.[21,40] The other parameters describing the mechano-biochemical properties of bonds are chosen to be F_b = 4 pN, $k_{on}^0 / k_0 = 10^4$ and l_{bind} = 1 nm, identical to those adopted in previous studies.[33,36] These selected values are used throughout our simulations unless specified otherwise, which are summarized together with the corresponding sources in **Table 1**.

3.2. Distribution of Bond Forces

To understand the role of loading conditions in controlling force distribution within the bond cluster, let us first consider the scenario where all 100 bonds remain closed. That is, their breaking rate is taken to be zero irrespective of the magnitude of forces acting on them. Numerical solutions to Equations 20 and 21 are obtained at three different values of anisotropy orientation, θ = 0°, 30° and 90°, under force-control loading condition. The total applied force is $N_T k_{LR} l_b$, corresponding to a nominal force $k_{LR} l_b$ per bond. As shown in **Figure 5**a, the applied load is significantly concentrated at the rim of adhesion in this case. Furthermore, the ratio of the maximum bond force to the average is found to be sensitive to the anisotropy orientation angle θ, a feature that can be understood by recalling that the so-called stress concentration index (SCI) strongly depends on the effective substrate rigidity.[10,11]

In the case of displacement-control loading, the imposed separation at the interface is chosen as $h = 2l_b$. As such, we intend to stretch each bond by the same amount as that in the force-control setup. However, due to the compliance of the substrate, most of the imposed deformation has actually been absorbed by the elastic medium and consequently, the level of bond forces, referring to Figure 5b, is much lower than that in Figure 5a. It is now clear that substrate compliance plays a key role in modulating the averaged level of bond forces if displacement loading condition is prescribed.

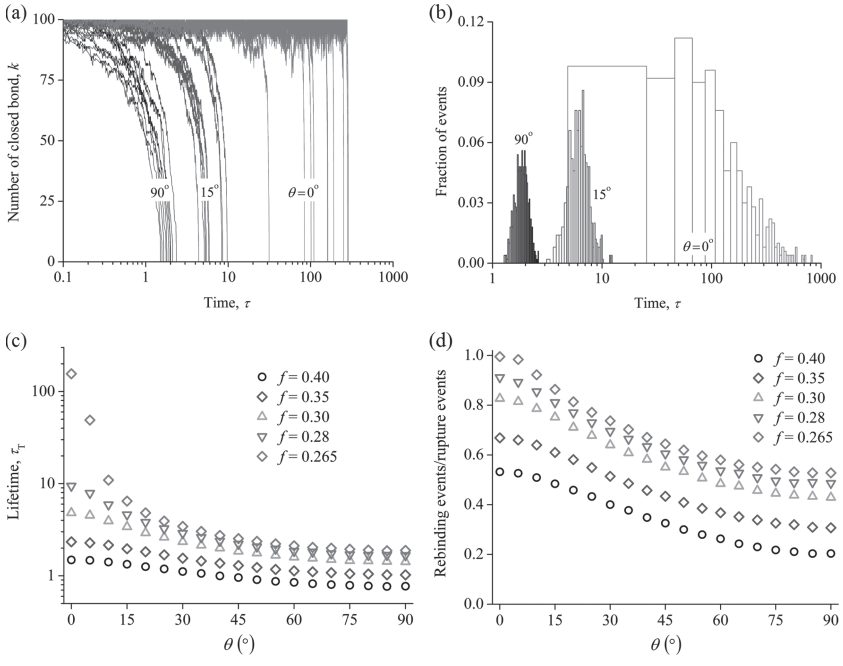

Figure 6. Effects of the anisotropy orientation angle θ on cluster stability when constant force is maintained. a) Single simulation trajectories of the closed bond number k versus elapsed time τ compared between different values of θ. 10 independent trials are plotted for each of the cases: $\theta = 0°$, 30° and 90°. b) Histograms of individual cluster lifetimes showing the fraction of adhesion failure events versus time τ for several values of θ. The level of nominal force per bond is fixed at $f = 0.265$ in (a,b). c) The cluster lifetime τ_T monotonically decreases as θ approaches 90° from zero for several levels of the nominal force per bond ($f = 0.4$, 0.35, 0.3, 0.28 and 0.265 from lower to upper curves). d) The averaged ratios of total events between bond rebinding and bond rupture as a function of θ for different levels of f.

3.3. Regulation of Anisotropy Orientation on Lifetime of Molecular Adhesion

Under the force-control setup, a remotely applied normal load F is kept constant throughout the simulation until the whole cluster is broken. In our analysis, it is more convenient to represent F in terms of a dimensionless nominal force per bond, denoted as f, through the relation $f = F/(N_t F_b)$. Once a bond is broken, the part of force originally shared by it must be transmitted to other close bonds. In other

words, the actual force per bond increases as more and more bonds become open. At a fixed load level of $f = 0.265$, **Figure 6**a plots 10 representative simulation trajectories of the number of closed bonds k versus time τ (real time normalized by $1/k_0$) for three values of θ. Clearly, k fluctuates around a plateau value close to N_t at the beginning but the adhesion abruptly loses its stability after a certain time, leading to catastrophic failure of all bonds. Each trajectory differs from others owing to the stochastic nature of bond rupture and rebinding. Nevertheless, collectively, the stability of adhesion clusters is found to be tightly regulated by the anisotropy orientation angle θ. Increasing substrate stiffness, or equivalently decreasing θ, leads to more stable clusters with longer lifetimes, as shown in Figure 6b where the histograms of a large number of simulation trials effectively produce the probability distribution of the observed failure of molecular adhesion. As the anisotropy orientation angle θ increases from zero to 90°, more failure events are shifted to the left, meaning more short-lived clusters, owing to the fact that stress concentration becomes more severe with elevated substrate compliance, referring to Figure 5a. The averaged cluster lifetime τ_T as a function of the anisotropy orientation angle θ at different levels of applied force f is depicted in Figure 6c. It can be seen that τ_T decreases monotonically with increasing θ (or equivalently increasing substrate compliance). A similar trend in the ratio of bond rebinding to rupture events has also been observed; see Figure 6d.

In direct contrast to the simulations where a constant force is maintained during bond evolution, we also consider a displacement-control setup in which the nominal separation h between the two surfaces is fixed. **Figure 7**a shows the cluster lifetime τ_T as a function of the anisotropy orientation angle θ for several specified values of H, defined through $H = h/l_b$. Not surprisingly, reducing the initial interfacial separation generally stabilizes the adhesion cluster. Intriguingly, the trend of adhesion lifetime depending on the anisotropy orientation here is opposite to that observed under the force-control condition. Specifically, the reduction in substrate rigidity induced by increasing θ results in a drop in the averaged force level among bonds, referring to Figure 5b. Furthermore, this effect of substrate softening on overall bond force alleviation seems to outweigh that caused by more concentrated stress, which ultimately leads to more stable adhesion. Figure 7b plots the ratio between bond rebinding and rupture events as a function of θ, which demonstrates an enhanced bond cooperativity through rebinding as the effective modulus of substrate decreases with increasing θ.

It is observed that for a given magnitude of load in any conditions, altering the anisotropy orientation angle θ, which may arise from remodeling processes in extracellular matrix or intracellular cytoskeleton or both, has profound effects in controlling the interfacial molecular adhesion. In fact, the adhesion lifetime can vary by orders of magnitude for modest θ-change of 15° or so (e.g., $f = 0.265$ in Figure 6c and $H = 18.5$ in Figure 7a). This is especially interesting in view that cells generally remodel cytoskeleton in interaction with an underlying substrate and immediately suggests a possible regulation mechanism by which cells can sensitively switch between long-survival and short-lived adhesion by adjusting stress fibers that leads to differently oriented material anisotropy.

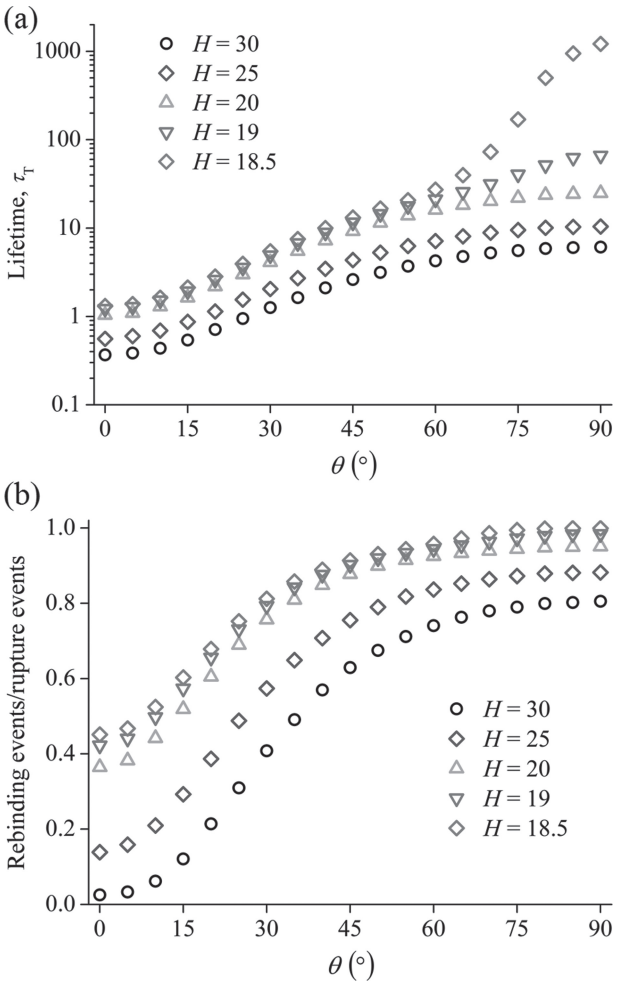

Figure 7. Effects of the anisotropy orientation angle θ on cluster stability when nominal interfacial separation is kept constant. a) The cluster lifetime τ_T monotonically increases as θ approaches 90° from zero for several values of the nominal interfacial separation (H = 30, 25, 20, 19 and 18.5 from lower to upper curves), with an anisotropy orientation dependence completely opposite to that in force-control setup. b) The averaged ratios of total events between bond rebinding and bond rupture as a function of θ for different prescribed values of H.

3.4. Viscoelastic Behavior of Receptor-Ligand Bond Cluster upon Stretching

The dynamic response of molecular bond clusters under stretching bears some similarities to viscous relaxation of a pulled dashpot. For the case of a constant applied force (force-control condition), the bond ensemble works against the applied load and impedes interfacial separation that depends on the instantaneous number of closed bonds. In the case of displacement-control loading, a varying level of reaction force maintains the imposed constant separation. Compared to how an ordinary dashpot behaves under pulling, the circumstance here is complicated by the feature of cluster failure at the interface, where the forced response of individual molecular bonds is stochastic and highly nonlinear, leading to varying impedance against constant stretching. **Figure 8**a,b plot 10 representative simulation

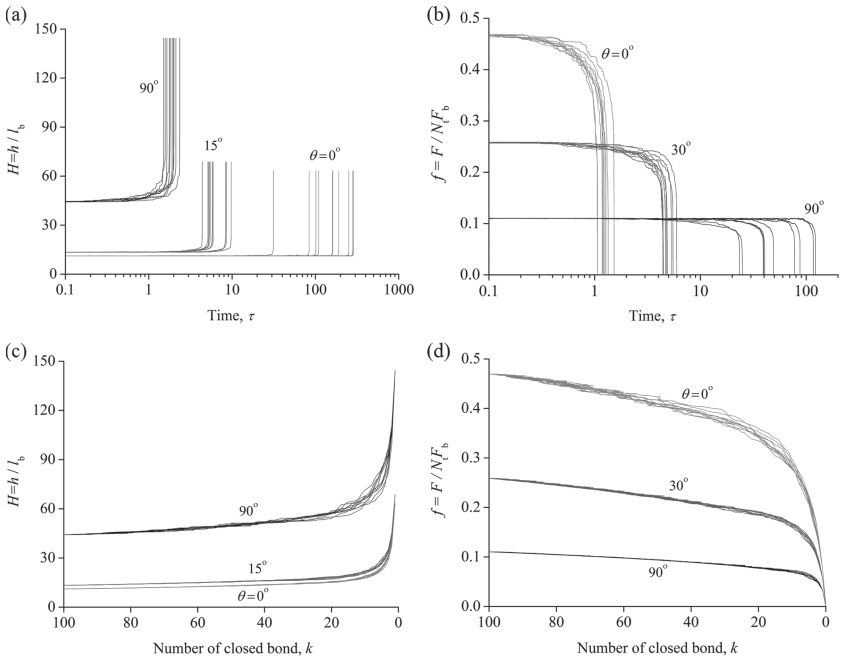

Figure 8. Time series of a) the nominal interfacial separation H for force-control systems and b) nominal force per bond f for displacement-control systems. 10 independents trials are plotted for each specified value of θ. Correlation between the instantaneous number of closed bonds k and c) the nominal interfacial separation H and d) the nominal force per bond f for the two loading conditions, respectively.

trajectories of the interfacial separation and reaction force with specified θ for the two types of loading conditions, respectively. Attributed to the feature of cascading bond failure after certain time points shown in Figure 6a, H for force-control systems, or f for displacement-control systems, fluctuates around a plateau value and suddenly diverges, or drops to zero, implying the accelerated process of bond breaking (Figure 8a,b, respectively). Any bond breaking weakens the molecular adhesion at the interface, so both H and f are tightly correlated to the instantaneous number of closed bond k as indicated in Figure 8c,d, respectively. Interestingly, the stochastic fluactuation in the relation of H (or f) versus k is dramatically reducd compared to the corresponding time-varying behavior in Figure 8a,b.

4. Conclusions

We have employed a stochastic-elasticity coupling framework to investigate the effects of transverse isotropy, a common form of material anisotropy in biological tissues, on the lifetime and stability of adhesive receptor-ligand bond clusters. The reversible processes of stochastic bond rupture and rebinding at molecular scale, together with the elastic response of transversely isotropic materials to bond force distributions at continuum scale, are integrated into a two-level computational model. It is shown analytically that under normal tractions, the elastic response of a transversely isotropic half-space, dependent on the anisotropic orientation, can be effectively represented by an isotropic counterpart. The results from Monte Carlo simulations show that, in general, the adhesive behavior of molecular bond clusters can be modulated by altering the anisotropy orientation of extracellular matrix or cytoskeleton, defined as the angle between the inherent orientation of material anisotropy and the interfacial plane where stochastic bond dissociation and association take place.

Upon the previous modeling on isotropic materials,[10–12] the progress this study made is the following: i) This work first shows that altering the anisotropy orientation of a transversely isotropic half-space can be reduced to an equivalent isotropic representation under the condition of normal surface loading. When the anisotropic half-space is subjected to nonzero traction in the direction tangential to its surface, the "isotropic equivalence" is no longer valid. ii) More importantly, this work indicates that cell-matrix adhesion can be effectively tuned by reorganizing the fibrous orientation of either cytoskeleton or substrate based on the same type of materials, which differs from existing isotropic studies where cell behaviors are influenced by changing the materials.

For two representative loading conditions, our results demonstrate that tailoring the microenvironment of cells with material anisotropy can significantly influence the collective binding of receptor-ligand molecules. Given the mounting evidence that cell spreading, orientation, migration, etc. can be directed by mechanical properties of the underlying enviroment, our approach may provide a promising route to effectively tune adhesion-mediated cellular behaviors via material anisotropy. Our results predict the opposite trends of the cluster lifetime as a function of the anisotropy orientation for two loading conditions. Thus, future measurements of the relation between anisotropy orientation of materials and stability of focal adhesions can provide a clue to distinguish whether constant levels of force or displacement are enforced in focal adhesion sites in an interplay among extracellular environments, receptor-ligand interactions and intracellular feedback processes of actomyosin contractility. For application of the present results, whether altering the anisotropy orientation in natural/artificial extracellular matrix tends to promote or diminish receptor-ligand bond clusters will rely on the actual loading condition at the cell-matrix interface.

Several important aspects of the problem have been idealized or neglected in the present study, which certainly warrant future investigation. First, we have limited our analysis to bond forces normal to the surface of an elastic substrate, and consequently the elastic response of a transversely isotropic medium can be represented by an isotropic counterpart via an effective modulus (Equation 14). When the cell-matrix interface is subjected to inclined loads where tangential force is significant,[47] the modeling in Section 2.3 needs to be extended to more general cases.[16,17,39] For another, we have assumed immobile receptor-ligand bonds at the cell-matrix interface, whereas diffusion-mediated bond recruiting and releasing of molecular

clusters are suspected to be important in discussing their temporal evolution and stability issue. In addition, the present study is carried out by assuming that the anisotropy orientation of materials (i.e., θ) is frozen during the lifetime of bond evolution, while there are interesting studies suggesting that anisotropy orientation of soft connective tissues, rooted in their fiber alignment at microscopic scales, changes over time in response to various external stimuli.[48,49] Moreover, it is believed that cells can remodel their cytoskeleton by reorganizing the orientation of stress fibers, which may lead to dynamic orientation of material anisotropy from intracellular side. For future study, it will be promising to pursue the complexities induced by dynamic remodeling of material anisotropy, where extra temporal scales in "live" materials emerge and interplay with the coordinated dynamics of molecular adhesion.

Acknowledgements

This work was supported by the "Thousand Young Talents Program" of China, the National Natural Science Foundation of China (No. 11202184), the Fundamental Research Funds for Central Universities (No. 2012QNA4023) of China, the Research Grants Council (Project No. HKU 7148/10E) of the Hong Kong Special Administration Region of China, and a seed fund (Project No. 201111159112) from the University of Hong Kong. H.G. gratefully acknowledges support from Zhejiang University through the Kuang-piu Visiting Chair Professorship and from the University of Hong Kong through the Distinguished Visiting Scholars Scheme (DVSS).

Received: January 8, 2013
Revised: February 13, 2013
Published online: April 8, 2013

[1] R. J. Pelham, Y. L. Wang, *Proc. Natl. Acad. Sci. USA* **1997**, *94*, 13661.
[2] C. M. Lo, H. B. Wang, M. Dembo, Y. L. Wang, *Biophys. J.* **2000**, *79*, 144.
[3] B. Cortese, G. Gigli, M. Riehle, *Adv. Funct. Mater.* **2009**, *19*, 2961.
[4] D. E. Discher, P. Janmey, Y. L. Wang, *Science* **2005**, *310*, 1139.
[5] A. J. Engler, S. Sen, H. L. Sweeney, D. E. Discher, *Cell* **2006**, *126*, 677.
[6] N. G. Genes, J. A. Rowley, D. J. Mooney, L. J. Bonassar, *Arch. Biochem. Biophys.* **2004**, *422*, 161.
[7] A. J. Engler, M. A. Griffin, S. Sen, C. G. Bonnetnann, H. L. Sweeney, D. E. Discher, *J. Cell Biol.* **2004**, *166*, 877.
[8] C. E. Chan, D. J. Odde, *Science* **2008**, *322*, 1687.
[9] S. Walcott, S. X. Sun, *Proc. Natl. Acad. Sci. USA* **2010**, *107*, 7757.
[10] J. Qian, J. Wang, H. Gao, *Langmuir* **2008**, *24*, 1262.
[11] J. Qian, J. Z. Wang, Y. Lin, H. J. Gao, *Biophys. J.* **2009**, *97*, 2438.
[12] J. Qian, H. J. Gao, *PLoS One* **2010**, *5*, e12342.
[13] S. C. Cowin, S. B. Doty, *Tissue Mechanics*, Springer, New York **2007**.
[14] T. T. Tower, M. R. Neidert, R. T. Tranquillo, *Ann. Biomed. Eng.* **2002**, *30*, 1221.
[15] K. P. Quinn, B. A. Winkelstein, *J. Biomech.* **2010**, *43*, 2637.
[16] S. H. Chen, H. J. Gao, *J. Mech. Phys. Solids* **2007**, *55*, 1001.
[17] H. Yao, S. Chen, P. R. Guduru, H. Gao, *Int. J. Solids Struct.* **2009**, *46*, 1167.
[18] H. J. Ding, W. Q. Chen, L. C. Zhang, *Elasticity of Transversely Isotropic Materials*, Springer, Dordrecht **2006**.
[19] F. Velardi, F. Fraternali, M. Angelillo, *Biomech. Modeling Mechanobiol.* **2006**, *5*, 53.
[20] X. N. Dong, X. E. Guo, *J. Biomech.* **2004**, *37*, 1281.
[21] D. A. Morrow, T. L. H. Donahue, G. M. Odegard, K. R. Kaufman, *J. Mech. Behav. Biomed. Mater.* **2010**, *3*, 124.
[22] M. Scherge, S. Gorb, *Biological Micro- and Nanotribology: Nature's Solutions*, Springer, Berlin **2001**.
[23] S. H. Hu, J. X. Chen, B. Fabry, Y. Numaguchi, A. Gouldstone, D. E. Ingber, J. J. Fredberg, J. P. Butler, N. Wang, *Am. J. Physiol.-Cell Physiol.* **2003**, *285*, C1082.
[24] T. G. Kim, H. Shin, D. W. Lim, *Adv. Funct. Mater.* **2012**, *22*, 2446.
[25] F. T. Moutos, L. E. Freed, F. Guilak, *Nat. Mater.* **2007**, *6*, 162.
[26] W. J. Li, R. L. Mauck, J. A. Cooper, X. N. Yuan, R. S. Tuan, *J. Biomech.* **2007**, *40*, 1686.
[27] T. M. Freyman, I. V. Yannas, R. Yokoo, L. J. Gibson, *Exp. Cell Res.* **2002**, *272*, 153.
[28] A. Saez, A. Buguin, P. Silberzan, B. Ladoux, *Biophys. J.* **2005**, *89*, L52.
[29] T. C. T. Ting, *Anisotropic Elasticity: Theory and Applications*, Oxford University Press, New York **1996**.
[30] R. De, A. Zemel, S. A. Safran, *Biophys. J.* **2008**, *94*, L29.
[31] R. De, A. Zemel, S. A. Safran, *Nat. Phys.* **2007**, *3*, 655.
[32] G. I. Bell, *Science* **1978**, *200*, 618.
[33] E. A. Evans, D. A. Calderwood, *Science* **2007**, *316*, 1148.
[34] T. Erdmann, U. S. Schwarz, *Phys. Rev. Lett.* **2004**, *92*, 108102.
[35] T. Erdmann, U. S. Schwarz, *J. Chem. Phys.* **2004**, *121*, 8997.
[36] H. J. Gao, J. Qian, B. Chen, *J. R. Soc. Interface* **2011**, *8*, 1217.
[37] T. Erdmann, U. S. Schwarz, *Biophys. J.* **2006**, *91*, L60.
[38] C. B. Hwu, *Eng. Fract. Mech.* **1993**, *45*, 89.
[39] X. Guo, F. Jin, *Int. J. Solids Struct.* **2009**, *46*, 3607.
[40] P. A. Sarma, R. M. Pidaparti, R. A. Meiss, *J. Biomed. Mater. Res. Part A* **2003**, *65A*, 1.
[41] K. L. Johnson, *Contact Mechanics*, Cambridge University Press, Cambridge **1985**.
[42] D. T. Gillespie, *J. Comput. Phys.* **1976**, *22*, 403.
[43] D. T. Gillespie, *J. Phys. Chem.* **1977**, *81*, 2340.
[44] E. Zamir, M. Katz, Y. Posen, N. Erez, K. M. Yamada, B. Z. Katz, S. Lin, D. C. Lin, A. Bershadsky, Z. Kam, B. Geiger, *Nat. Cell Biol.* **2000**, *2*, 191.
[45] N. Q. Balaban, U. S. Schwarz, D. Riveline, P. Goichberg, G. Tzur, I. Sabanay, D. Mahalu, S. Safran, A. Bershadsky, L. Addadi, B. Geiger, *Nat. Cell Biol.* **2001**, *3*, 466.
[46] M. Arnold, E. A. Cavalcanti-Adam, R. Glass, J. Blummel, W. Eck, M. Kantlehner, H. Kessler, J. P. Spatz, *ChemPhysChem* **2004**, *5*, 383.
[47] K. D. Chen, Y. S. Li, M. Kim, S. Li, S. Yuan, S. Chien, J. Y. J. Shyy, *J. Biol. Chem.* **1999**, *274*, 18393.
[48] E. Kuhl, K. Garikipati, E. M. Arruda, K. Grosh, *J. Mech. Phys. Solids* **2005**, *53*, 1552.
[49] N. J. B. Driessen, G. W. M. Peters, J. M. Huyghe, C. V. C. Bouten, F. P. T. Baaijens, *J. Biomech.* **2003**, *36*, 1151.